Dissipative solitons in photonic molecules

(article starts on next page)

Dissipative solitons in photonic molecules

Óskar B. Helgason, Francisco R. Arteaga-Sierra, Zhichao Ye, Krishna Twayana, Peter A. Andrekson, Magnus Karlsson, Jochen Schröder and Victor Torres-Company*

Department of Microtechnology and Nanoscience, Chalmers University of Technology, 41296 Gothenburg, Sweden

* Correspondence to: torresv@chalmers.se

Many physical systems display quantized energy states. In optics, interacting resonant cavities show a transmission spectrum with split eigenfrequencies, similar to the split energy levels that result from interacting states in bonded multi-atomic, i.e. molecular, systems. Here, we study the nonlinear dynamics of photonic diatomic molecules in linearly coupled microresonators and demonstrate that the system supports the formation of self-enforcing solitary waves when a laser is tuned across a split energy level. The output corresponds to a frequency comb (microcomb) whose characteristics in terms of power spectral distribution are unattainable in single-mode (atomic) systems. Photonic molecule microcombs are coherent, reproducible, and reach high conversion efficiency and spectral flatness whilst operated with a laser power of a few milliwatts. These properties can favour the heterogeneous integration of microcombs with semiconductor laser technology and facilitate applications in optical communications, spectroscopy and astronomy.

Optical microresonators are microscale cavities that confine light by resonant recirculation. They can be arranged in coupled arrays, with the dimensions of the unit cell precisely engineered by means of lithography. These coupled microresonator arrays exhibit characteristics that are analogous to the electron dynamics in strongly correlated many-body systems, allowing to study exotic states of matter whose Hamiltonians are difficult to access in their natural environment[1-4].

Small-volume optical microresonators with high quality-factors (Q-factors) lead to a large build-up of the intra-cavity intensity, easing the observation of optical nonlinear phenomena with low-power continuous-wave lasers[5,6]. A canonical example is the formation of dissipative solitons (DSs)[7] – self-

enforcing solitary waves in nonlinear dissipative systems subject to an external energy supply[8,9]. DSs exist in cavities with normal as well as anomalous dispersion and exhibit a rich diversity of soliton dynamics[10-15]. In the time-domain, a DS corresponds to a localized waveform circulating at a rate commensurate to the cavity free-spectral-range (FSR)[7]. From a practical perspective, DSs in microresonators provide the means to realize microcombs[8] and a chip-scale version of the bi-directional coherent link between optics and microwave references that is the cornerstone of contemporary frequency metrology[16].

Most investigations of optical DSs in cavities have been carried out in the anomalous dispersion regime, where fundamental nonlinear physics[17] precludes attaining microcombs with an efficient distribution of the power available from the laser pump. In the normal dispersion regime, DSs can exist in the form of interlocked switching waves that connect the homogeneous steady-state solutions of the nonlinear bistability diagram[11,18]. These waveforms feature high power-conversion efficiency[19] but their accessibility is limited to a narrow existence range of design and control parameters that are difficult to satisfy in single-transverse mode (i.e. single-mode) cavities. These limits are intrinsic to single-mode dynamics and irrespective of the Q factor or nonlinear coefficient of the cavity. Here, we investigate DS dynamics in a set of two linearly coupled high-Q silicon nitride microresonators (Fig. 1). The microresonators have identical cross-section geometry but different FSRs. The dispersion of the fundamental mode in the cavities is normal, resulting in a decreasing FSR with optical frequency. In absence of coupling, the resonant frequencies of the cavities, $\omega_\mu^{(a)}$ and $\omega_\mu^{(b)}$, are $\omega_\mu^{(a,b)} = \omega_0^{(a,b)} + \mu D_1^{(a,b)} + \mu^2 D_2^{(a,b)}/2 + \ldots$, with $D_1^{(a,b)}/(2\pi)$ representing the FSR of the cavity (a,b), $D_2^{(a,b)}/(2\pi)$ the dispersion parameter that accounts for the deviation from a grid of evenly spaced frequencies, and μ is an integer number. Frequencies that satisfy $\omega_m^{(a)} = \omega_n^{(b)}$ are degenerate so that a laser tuned to one of them would be resonant in both cavities, where n and m are integer numbers. By placing the microresonators in close proximity, the evanescent field of one cavity serves as a perturbation to the field in the adjacent one, resulting in linear coupling. The coupling lifts the frequency degeneracy and manifests in the emergence of a doublet of two new eigenfrequencies, corresponding to the eigenvalues of the supermodes. Assuming negligible impact from losses, the supermodes are located at $\omega^{(s,as)} = \left[\omega_m^{(a)} + \omega_n^{(b)}\right]/2 \pm \left\{\left[\omega_m^{(a)} - \omega_n^{(b)}\right]^2/4 + |\kappa|^2\right\}^{1/2}$ with κ being the coupling rate between

microresonators. This arrangement of two microresonators placed in close proximity is often called "photonic molecule" in analogy to a diatomic multi-level system[20]. Our photonic molecule offers the flexibility of tuning the frequency offset $\omega_0^{(a)}$ via the thermo-optic effect by placing a heater on top of one of the microresonators. This in turn permits continuous tuning of the location of the degeneracy point $\omega_m^{(a)} = \omega_n^{(b)}$ and hence the frequency separation of the doublet $\omega^{(s)} = \omega^{(as)}$. The ability to lift the frequency degeneracy in linearly coupled nonlinear cavities has been used previously to impedance match the microcomb with an auxiliary drop port[21], as well as to facilitate phase matching with the pump frequency mode and initiate microcombs via modulation instability in the normal dispersion regime[22-24]. Our study (Fig. 2) unveils the role of the coupling coefficient as the key mechanism to broaden the existence area of DSs, allowing to deterministically access coherent microcombs by pumping the split energy level. These results elucidate the DS dynamics in normal dispersion photonic molecules, providing clear guidelines for their design and operation.
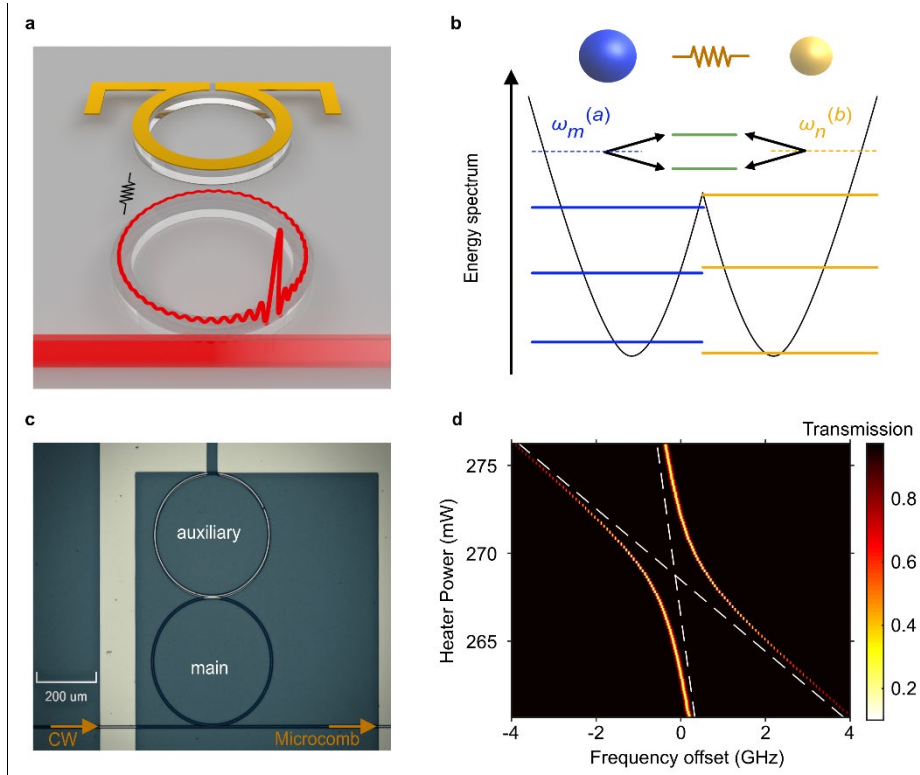

Fig. 1. Photonic molecule based on linearly coupled microresonators. (**a**) Artist rendition of a dissipative soliton generated in a photonic molecule, where coupling between microresonators is induced by placing them in close proximity. A heater on top of the auxiliary microresonator controls the frequency location of the degeneracy point. The coupling induces a controllable split resonance at this location, similar to a split energy level in a diatomic molecule (**b**). (**c**) Photograph of one of the fabricated photonic molecule devices. (**d**) Measurement of the frequency split as a function of heater power, illustrating the coupling

between resonant frequencies. The auxiliary resonance shifts diagonally across the map, generating two supermodes as it gets more coupled to the main resonance. The main resonance shifts slightly with heater power due to thermal crosstalk.

Results

Dissipative soliton dynamics in photonic molecules

In continuous-wave-pumped optical microresonators, DSs exist in the two-dimensional space given by the pump power and frequency detuning[25,26]. The existence range of DSs is rather narrow in normal-dispersion microresonators supporting a single transverse mode[26], as indicated by the area delimited by the solid black curve in Fig. 2. In a photonic molecule with fixed coupling rate (see parameters and simulation approach in Methods), DSs exist in the region corresponding to the blue shade. A number of important characteristics can be noted. First, this area is significantly broader than for the single-mode case, aiding the experimental accessibility of DSs. The simulations in Fig. 2 are conducted considering first-order-dispersion walk-off between the two microresonators. Photonic molecules enable the existence of asymmetric waveforms in both frequency and time domains that are not a steady-state solution of single-mode systems. Second, the DS dynamics in photonic molecules also leads to breathers and other forms of unstable waveforms, which have been previously encountered in normal-dispersion cavities[27]. These regions of instability can be avoided if the level of the pump power is properly selected, allowing the transit into the stable DS regime by simply tuning the laser at constant power into the doublet frequency starting from the blue side. This way, the DS regime can be accessed in a deterministic manner at constant power after transiting through an initial stage of modulation instability, followed by the formation of Turing rolls, as can be seen from points marked as 1 and 2 in Fig. 2. When a Turing roll is generated in the main cavity, another weakly oscillating waveform arises in the auxiliary cavity through linear coupling. The transition to the DS regime from the Turing rolls is accompanied by an abrupt decrease in intracavity power in the auxiliary cavity (see Supplementary Information), and the existence areas for these types of waveforms are clearly distinguished in the two-dimensional map. Finally, point 3 in the diagram illustrates the final states and compares the simulation (blue) with the measured microcomb spectrum (red). The detuning in point 3 was determined qualitatively from measurements (see Supplementary Information). The steady-state time-domain waveform corresponds to a pulse with strong oscillations at the bottom, different to the sech profile encountered in anomalous dispersion cavities[7,9]. The high-power level is not a constant plateau either, as is common with dark-pulse Kerr combs or

platicons[11,28]. The oscillations are a consistent feature among DSs in single-mode normal-dispersion microcombs, previously described as an interlock between the oscillatory tails of two switching waves, that keeps the waveform from collapsing[18]. A crucial difference in these photonic molecule DSs is that the power levels of the intracavity waveform do not correspond to the steady-state solutions of the multi-stability curve, as shown in Fig. 2c and analysed in more detailed in the Supplementary Information. The auxiliary cavity features another solitary wave synchronized to the pulse of the main cavity whose origin can be ascribed to the linear coupling and not the intrinsic Kerr nonlinearity of the auxiliary cavity. Interestingly the kinks at the trailing edge of the pulse of the two waves in the cavities are in phase, but the leading edge appears exactly out of phase with the main cavity waveform. The measured repetition rate for the waveform in point 3 is illustrated in Fig. 2d and it points to a coherent and stable waveform. Our study indicates the DS dynamics in photonic molecules is predictable and can be adequately reproduced using our numerical model after retrieving the parameters of the coupled cavities by absorption spectroscopy[29].
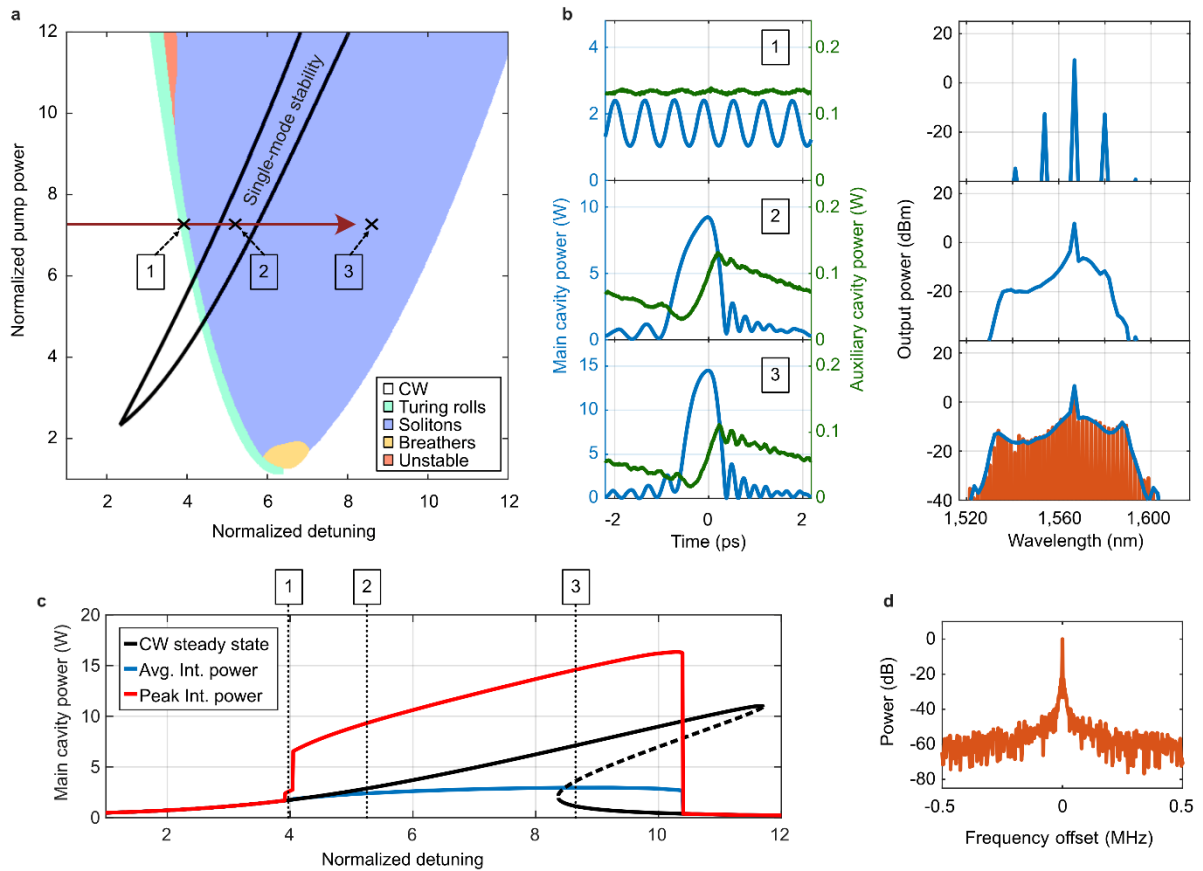

Fig. 2. DS dynamics in photonic molecules. (a) Simulation of the stability chart of a photonic molecule in the normal-dispersion regime with fixed coupling rate (730 MHz). The FSR is 227.33 GHz and 236.84 GHz for the main and auxiliary

cavity, respectively. The pump power and detuning are normalized as in ref. [25]. (**b**) Simulated waveforms in points 1, 2 and 3 appear in the time domain (left column) and frequency domain (right column). Point 3 compares the spectrum of simulations (blue) with measurements (red). (**c**) Simulated evolution of the average intracavity power and peak intracavity power for main cavity as the laser is tuned into resonance. It also shows the calculated CW steady-state solutions for the photonic molecule. The locations of the microcombs in (**b**) are depicted by the vertical dashed lines. (**d**) The beat note of the line spacing for the measured microcomb in point 3.
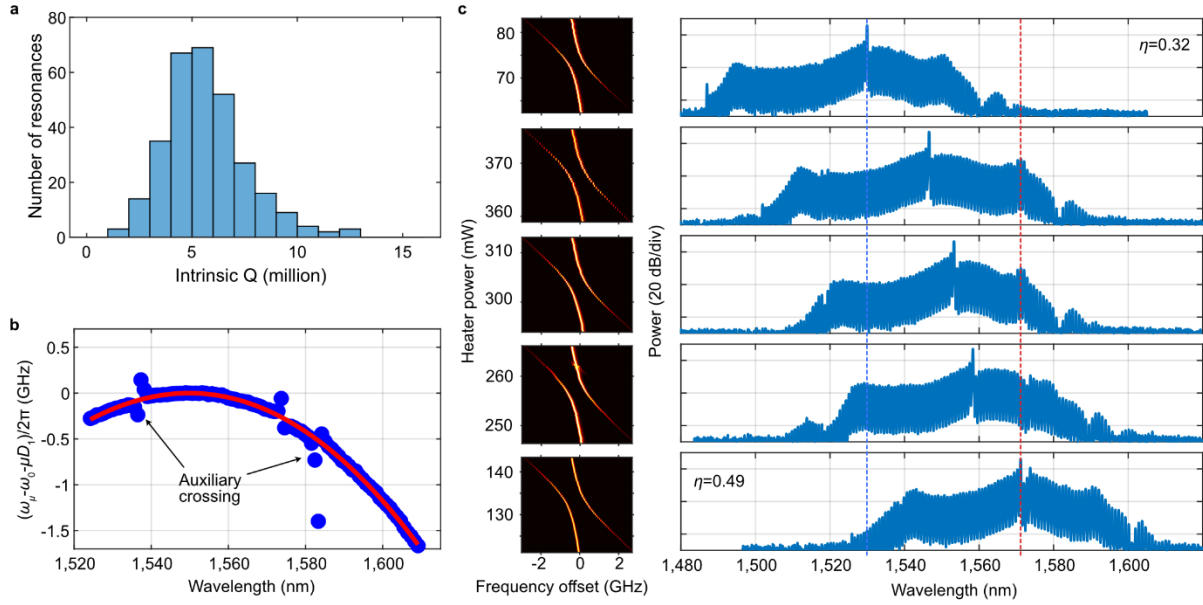

Fig. 3. Control of photonic molecules and tuneable microcombs. (**a**) Statistical analysis of the intrinsic Q factor of 3 nominally identical devices. The mean intrinsic value is 5.7 million. (**b**) Integrated dispersion of the main cavity mode, illustrating two split resonances (marked as auxiliary crossing points) that result from the coupling to the auxiliary cavity. The FSR is 104.84 GHz and 106.9 GHz for the main and auxiliary cavity, respectively. (**c**) The frequency location of the crossing points can be selected with the heater power, and by tuning the pump laser to this location, wavelength tuneable microcombs are generated. The dashed vertical lines indicate the centre wavelength location of the initial and final comb states.

Tuneable photonic molecule microcombs

Our photonic molecules are fabricated using a subtractive processing method for silicon nitride[30]. With this technique we can fabricate dispersion-engineered microring resonators with high optical-field confinement. The fabrication process results in reproducible photonic molecules, as illustrated by the statistical analysis of the intrinsic Q presented in Fig. 3a for multiple resonances analysed in the 1.5 µm band for 3 devices with identical geometry. The mean Q value is about an order of magnitude higher compared to previously reported microcombs generated in normal-dispersion silicon nitride

photonic molecules[22]. Note that these devices have a longer cavity compared to the example in Fig. 2, resulting in an FSR of nearly 105 GHz. The dispersion of the fundamental transverse mode in the main cavity mode is normal, as illustrated in Fig. 3b. This figure also shows two avoided mode crossings at 1,535 nm and 1,585 nm due to the controllable coupling between microresonators. In addition, there is an avoided mode crossing at 1,572 nm owing to coupling between the fundamental transverse mode to a higher-order mode in the same microresonator, but this has only a minor influence on the results. The ability to select the frequency location of the split resonance results in broadly tuneable DS microcombs by frequency matching the pump laser to the location of the split energy level of the photonic molecule. This is shown in Fig. 3c, where we tune the photonic molecule microcombs over 40 nm within the telecommunications C band, from 1,530 to 1,570 nm, while maintaining an almost constant pump power (13 mW at the short wavelength and 18 mW near 1,570 nm). The main cavity is over-coupled (with extrinsic Q factor, Q_{ex}=2-4 million), resulting in a situation closer to effective critical coupling (loss rate equals coupling rate) when the DS is generated.

Pulse measurement

We conducted time-domain measurements of these microcomb states using an optical sampling oscilloscope. We used the device demonstrated in Fig. 3, pumped with nearly 18 mW of on-chip power at 1,546.7 nm. The corresponding optical spectrum and radio-frequency amplitude noise are displayed in Fig. 4a-b, providing further evidence of the low-noise state of our microcombs. Using the measured parameters of the photonic molecule, we matched the measured microcomb in simulations, and the time-domain signal indicates that a single DS is circulating in the main cavity (see Fig. 4c). This DS is outcoupled to the bus waveguide and it gets distorted due to the coherent superposition with the fraction of the continuous-wave laser that is uncoupled to the photonic molecule, with the expected waveform depicted in Fig. 4d. The trace measured by the oscilloscope is shown in Fig. 4e. The limited temporal resolution of the oscilloscope does not allow to resolve the fast oscillations of the soliton waveform, but it provides a qualitative estimate of the pulsed nature of the photonic molecule microcomb, revealing the asymmetry in time domain and a duty cycle below 50%.

Conversion efficiency and flatness of photonic molecule microcombs

Next, we investigate the power conversion efficiency of photonic molecule microcombs. DSs in normal-dispersion microresonators have the ability to transform a larger fraction of the pump laser's power into useful comb power[19], a metric that is quantified by the conversion efficiency (defined as the ratio between on-chip output power excluding the pump divided by the input pump power). Over the frequency span displayed in Fig. 3c, the conversion efficiency, η, increases from 32% to 49%. The increase in conversion efficiency is consistent with our simulations (see Supplementary Information), and it is mainly caused by the increase in coupling rate at long wavelengths. Reaching such a high conversion efficiency is beneficial in several applications of microcombs, but it can be misleading, since it is often dominated by the comb power concentrated in just a few lines, resulting in microcomb spectra with a non-smooth envelope. Having a uniform power distribution is important when employing microcombs for coherent optical communications[31,32], the calibration of astronomical spectrographs[33] or dual-comb spectroscopy[34]. The results in Fig. 3 indicate that microcombs generated in photonic molecules result in an improved balance between conversion efficiency and spectral distribution. In the Supplementary Information, we quantify these improvements by analysing the net conversion efficiency, demonstrating a 6-18 times increase compared to state of the art microcombs. A similar combination of conversion efficiency and spectral distribution can be found in the designs in Fig. 2 as well. Here, we take advantage of the increased existence regime at lower pump power, generating the comb from 2.5 mW on-chip power (see Fig. 5). This power level is compatible with recent advances in heterogeneous integration of III-V lasers on silicon nitride[35]. The conversion efficiency is 36% resulting in a power per line > 12 μW, with little variation across the spectrum. Such a combination of spectral flatness, high power conversion efficiency and low pump power operation is unprecedented in microcombs.
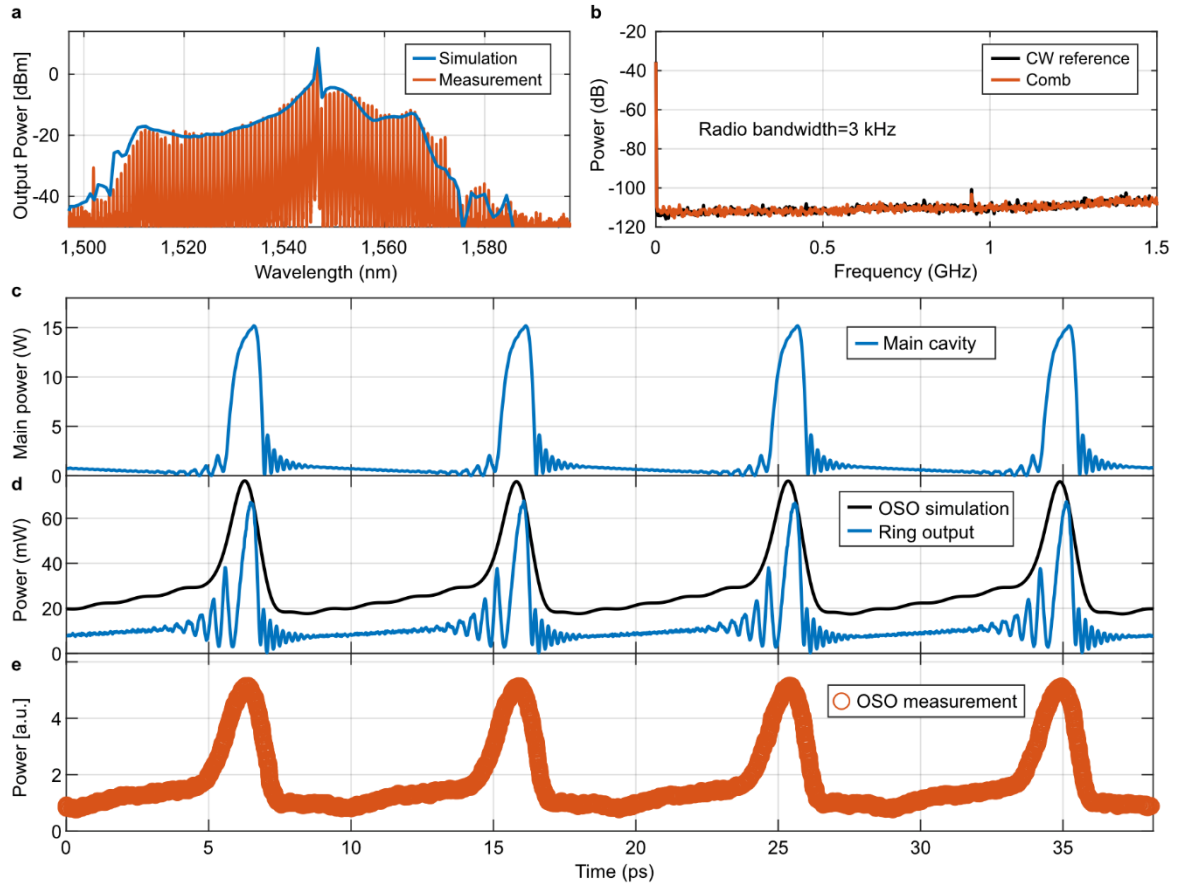
Fig. 4. Temporal measurement of a photonic molecule microcomb. (**a**) Microcomb spectrum along with the simulation results. (**b**) Low-frequency amplitude noise spectrum of the microcomb measured in a photodiode. The trace does not deviate from the measured continuous-wave (CW) reference, thus confirming a low-noise microcomb state. (**c**) Simulated intracavity power in the main cavity spanning four periods. (**d**) Simulated dissipative solitons at the outcoupled bus waveguide (blue). The black trace simulates the expected waveform as it would be captured by an optical sampling oscilloscope (OSO) with limited bandwidth. (**e**) Output of the photonic molecule measured in an OSO with 1 ps temporal resolution.
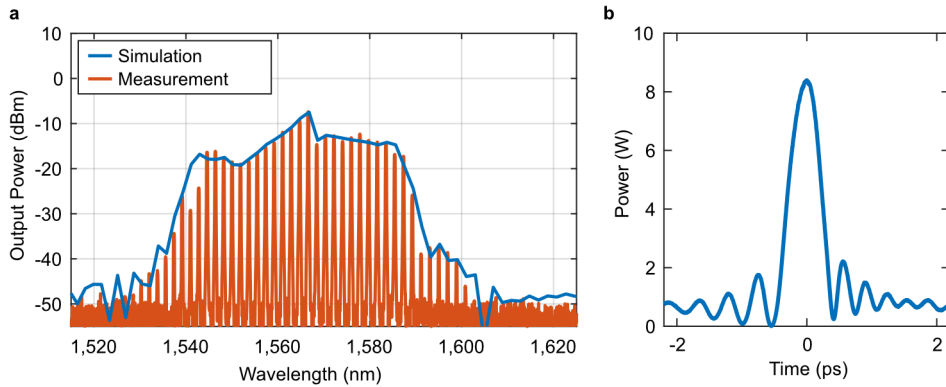

Fig. 5. Relatively flat photonic molecule microcombs. (**a**) Measured on-chip power spectrum and (**b**) simulated time domain intensity profile inside the cavity. The comb is initiated by tuning the laser into main resonance from the blue side, while the auxiliary mode is blue detuned by 3 GHz from the main resonance.

9

Discussion

We have demonstrated the formation of dissipative solitons in photonic diatomic molecules implemented in linearly-coupled normal-dispersion microresonators. The coupling rate between microresonators gives an additional degree of freedom for the synthesis of soliton states, expanding their existence range in the pump power–detuning bidimensional space with respect to a single mode (atomic) system. We demonstrate access to soliton states with high conversion efficiency and uniform power distribution, whose dynamics can be accurately predicted using the linear parameters of the cold molecular ensemble. The low-power operation makes photonic molecule microcombs well suited for heterogeneous integration with semiconductor lasers, and their power efficiency and uniform distribution can be particularly useful for applications such as optical communications.

Data availability

The raw data used in this work, including the raw figure data, can be accessed at xxxxxxx.

References

1. Hodaei, H., Miri, M.-A., Heinrich, M., Christodoulides, D.N. & Khajavikhan, M. Parity-time-symmetric microring lasers. *Science* **346**, 975-978 (2014).

2. Peng, B. *et al*. Loss-induced suppression and revival of lasing. *Science* **346**, 328-332 (2014).

3. Bandres, M.A. *et al.* Topological insulator laser: experiments. *Science* **359**, eaar4005 (2018).

4. Zhang, M. *et al.* Electronically programmable photonic molecule. *Nature Photon.* **13**, 36-40 (2019).

5. Ferrera, M. *et al.* Low-power continuous-wave nonlinear optics in doped silica glass integrated waveguide structures. *Nature Photon.* **2**, 737-740 (2008).

6. Lu, X. *et al.* Efficient telecom-to-visible spectral translation through ultralow power nonlinear nanophotonics. *Nature Photon.* **13**, 593-601 (2019).

7. Herr, T. *et al*. Temporal solitons in optical microresonators. *Nature Photon.* **8**, 145-152 (2014).

8. Kippenberg, T.J., Gaeta, A.L., Lipson, M., & Gorodetsky, M.L. Dissipative Kerr solitons in optical microresonators. *Science* **361**, eaan8083–13 (2018).

9. Leo, F. *et al.* Temporal cavity solitons in one-dimensional Kerr media as bits in an all-optical buffer. *Nature Photon.* **4**, 471-476 (2010).

10. Brasch, V. *et al.* Photonic chip-based optical frequency comb using soliton Cherenkov radiation. *Science* **351**, 357-360 (2015).

11. Xue, X. *et al.* Mode-locked dark pulse Kerr combs in normal-dispersion microresonators. *Nature Photon.* **9**, 594-600 (2015).

12. Bao, C. *et al.* Observation of Fermi-Pasta-Ulam recurrence induced by breather solitons in an optical microresonator. *Phys. Rev. Lett.* **117**, 163901 (2016).

13. Cole, D.C., Lamb, E.S., Del'Haye, P., Diddams, S.A. & Papp, S.B. Soliton crystals in Kerr resonators. *Nature Photon.* **11**, 671-676 (2017).

14. Guo, H. *et al.* Universal dynamics and deterministic switching of dissipative Kerr solitons in optical microresonators. *Nature Phys.* **13**, 94-102 (2017).

15. Nazemosadat, E. *et al.* Switching dynamics of dark-pulse Kerr comb states in optical microresonators. Preprint at https://arxiv.org/abs/1910.11035 (2019)

16. Spencer, D.T. *et al.* An optical-frequency synthesizer using integrated photonics. *Nature* **557**, 81-85 (2018).

17. Bao, C. *et al.* Nonlinear conversion efficiency in Kerr frequency comb generation. *Opt. Lett.* **39**, 6126-6129 (2014).

18. Parra-Rivas, P., Gomila, D., Knobloch, E., Coen, S. & Gelens, L. Origin and stability of dark pulse Kerr combs in normal dispersion resonators. Opt. Lett. **41**, 2402-2405 (2016).

19. Xue, X., Wang, P.-H., Xuan, Y., Qi, M., & Weiner, A.M. Microresonator Kerr frequency combs with high conversion efficiency. *Laser & Photon. Rev.* **11**, 1600276 (2017).

20. Liao, K. *et al.* Photonic molecule quantum optics. *Adv. Opt. Photon.* **12**, 60-134 (2020).

21. Xue, X., Zheng, X. & Zhou, B. Super-efficient temporal solitons in mutually coupled optical cavities. *Nature Photon.* **13**, 616-622 (2019).

22. Xue, X. *et al.* Normal-dispersion microcombs enabled by controllable mode interactions. *Laser & Photon. Rev.* **9**, 23-28 (2015).

23. Kim, B.Y. *et al.* Turn-key, high-efficiency Kerr comb source. *Opt. Lett.*, **44**, 4475-4478 (2019).

24. Fuji, S. *et al.* Analysis of mode coupling assisted Kerr comb generation in normal dispersion system. *IEEE Photon. J.* **10**, 4501511 (2018).

25. Coen, S. & Erkintalo, M. Universal scaling laws of Kerr frequency combs. *Opt. Lett.* **38**, 1790-1792 (2013).

26. Godey, C., Balakireva, I.V., Coillet, A. & Chembo, Y.K. Stability analysis of the spatiotemporal Lugiato-Lefever model for Kerr optical frequency combs in the anomalous and normal dispersion regimes. *Phys. Rev. A* **89**, 063814 (2014).

27. Bao, C. *et al.* Observation of Breathing Dark Pulses in Normal Dispersion Optical Microresonators. Phys. Rev. Lett. **121**, 257401 (2018).

28. Lobanov, V.E., Lihachev, G., Kippenberg, T.J. & Gorodetsky, M.L. Frequency combs and platicons in optical microresonators with normal GVD. *Opt. Express* **23**, 7713-7721 (2015).

29. Del'Haye, P., Arcizet, O., Gorodetsky, M.L., Holzwarth, R. & Kippenberg, T.J. Frequency comb assisted diode laser spectroscopy for measurement of microcavity dispersion. *Nature Photon.* **3**, 529-533 (2009).

30. Ye, Z., Twayana, K., Andrekson, P.A. & Torres-Company, V. High-Q Si_3N_4 microresonators based on a subtractive processing for Kerr nonlinear optics. *Opt. Express* **27**, 35719-35727 (2019).

31. Fülöp, A. *et al.* High-order coherent communications using mode-locked dark-pulse Kerr combs from microresonators. *Nature Comm.* **9**, 1598 (2018).

32. Marin-Palomo, P. *et al.* Microresonator-based solitons for massively parallel coherent optical communications. *Nature* **546**, 274-279 (2017).

33. Suh, M.-G. *et al.* Searching for exoplanets using a microresonator astrocomb. *Nature Photon.* **13**, 25-30 (2019).

34. Suh, M.-G., Yang, Q.F., Yang, K.Y., Yi, X. & Vahala, K.J. Microresonator soliton dual-comb spectroscopy. *Science* **354**, 600-603 (2016).

35. Xiang, C. *et al.* Narrow-linewidth III-V/Si/Si₃N₄ laser using multilayer heterogeneous integration. *Optica* **7**, 20-21 (2020).

36. Fülöp, A. *et al*. Active feedback stabilization of normal-dispersion microresonator combs. *European Conference on Lasers and Electro-Optics and European Quantum Electronics Conference*, paper *CD-P.45* (2017)

37. Del'Haye, P., Papp, S.B. & Diddams, S.A. Hybrid electro-optically modulated microcombs. *Phys. Rev. Lett.* **109**, 263901 (2012).

38. Andrekson, P.A. & Westlund, M. Nonlinear optical fiber based high resolution all-optical waveform sampling. *Laser & Photon. Rev.* **1**, 231-248 (2007).

39. Hult, J. "A Fourth-Order Runge–Kutta in the Interaction Picture Method for Simulating Supercontinuum Generation in Optical Fibers. *Journal of Lightwave Technology*, **25**, 3770-3775 (2007).

Contributions

ÓBH conducted the experiments and wrote the code for simulating photonic molecule solitons and managed a portion of the simulations. FRAS ran cluster simulations and characterized the simulated microcombs to generate existence maps. ZY fabricated the devices. KT provided the setup and code to characterize the dispersion and quality factors of the devices. ÓBH, FRAS, PAA, MK, JS and VTC contributed in terms of analysis and interpretation of the data. VTC, ÓBH and FRAS prepared the manuscript with input from all co-authors.

Competing interests

The authors declare no competing interests

Methods

Device Characteristics

The two devices described in the main text were fabricated in silicon nitride using a subtractive processing method[30], with a microheater placed on the auxiliary cavity. The waveguides of both cavities for both devices are designed with a height of 600 nm and 1,650 nm width. Device 1 is presented in Fig. 2 and Fig. 5. It has a main ring with radius of 100 μm and auxiliary ring of radius=96 μm. The Device 2, presented in Figs. 3 and 4, has a main ring with radius=217 μm and an auxiliary

ring of radius=213 μm. The dispersion and linewidth parameters of both devices were measured with the method described in ref. [27] and the Supplementary Information.

Device 1 was characterized at centre wavelength 1566.8 nm to have FSR_{main}=227.32 GHz, FSR_{aux}=236.7 GHz, $D_2/2\pi$=−3 MHz, $D_3/2\pi$=89 kHz and $\kappa/2\pi$=730 MHz, where $D_3/2\pi$ is the third-order dispersion. The intrinsic and extrinsic quality factors are Q_i=7.5 million and Q_{ex}=3.8 million.

Device 2 was characterized at centre wavelength 1,550 nm to have FSR_{main}=104.84 GHz, FSR_{aux}=106.9 GHz, $D_2/2\pi$=−0.6 MHz, $D_3/2\pi$=3 kHz and $\kappa/2\pi$=485 MHz. The intrinsic and extrinsic quality factors are Q_i=5.7 million and Q_{ex}=3.1 million. The nonlinear Kerr parameter is found using a mode-solver for the waveguide cross-section and materials as γ=1.1 (Wm)$^{-1}$. The Q-factor and group velocity dispersion of the auxiliary cavity were not directly measured but assumed to be the same as in the main cavity. This is a fair assumption since both cavities have the same cross-sectional design. More details about these parameters are provided in the Supplementary Information.

Microcomb operation

The chip containing the microresonator was placed on a thermally stabilized metal plate. Light was coupled into the bus waveguide at the facets of the chip via lensed fibres, carefully placed using piezo controlled positioning stages. The fraction of optical power lost at each facet was roughly 2.5 dB. The light was provided by a tuneable external cavity diode laser (ECDL). The heater circuit of the auxiliary ring was placed on the surface of the chip. It was accessed by placing micro positioned DC probes on the surface contacts. The voltage applied to the heater circuit shifts the location of the longitudinal modes in the auxiliary cavity. The location of the mode-crossing was tuned by changing the applied voltage.

To generate a DS, the auxiliary heater was tuned such that the auxiliary resonance was slightly blue detuned from the main resonance (i.e. $\omega_0^{aux}>\omega_0^{main}$). The comb was generated deterministically by simply tuning the ECDL from the blue side into the main resonance. Photonic molecule microcombs appear to be thermally self-stabilized, but the cases that deal with low pump power required a feedback to stabilize the ECDL wavelength by locking the comb power to a fixed level[36]. In the case of Fig. 3, once a comb state was achieved, the shape of the comb was further optimized by tuning both the heater and the laser frequency. An illustration of the DS initiation is provided in the Supplementary Information.

Repetition rate measurements

The repetition rate of the microcomb displayed in Fig. 2b was measured by electro-optic down conversion[37]. The microcomb was driven by the ECDL, then modulated with a phase modulator (PM) with frequency f_{RF}=25.146 GHz, generating a sub-comb around each line of the microcomb. The radio frequency (RF) power supplied to the PM was sufficiently high such that the sub-combs overlap. The modulated microcomb was then filtered in an optical programmable filter (OPF), set to provide equally spaced band-pass filters, with a 0.3 nm passband and separation equal to the cavity FSR. Thus, only the desired overlapping lines of the sub-combs were measured, beating together in a high-speed photodiode before being recorded in a high-speed real-time sampling oscilloscope. The measurement spanned 0.4 ms which corresponds to a resolution bandwidth of 2.5 kHz. Finally, the beat note was retrieved via simple Fourier analysis. A schematic and further details are provided in the Supplementary Information.

Measurement of pulses

The pulses at the output of our photonic molecule were measured by connecting directly the outcoupled light into a commercial optical sampling oscilloscope (OSO) with ~1 ps temporal resolution. The OSO operates within 1,525-1,565 nm, filtering away all components outside of that band. It records the temporal signal via nonlinear gating in a highly nonlinear fibre using a sub picosecond laser pulse[38]. The OSO simulation in Fig. 4d includes the dispersion introduced by a 1 m fibre patchcord and bandpass filtering to emulate the response of the oscilloscope.

Numerical simulations

A numerical verification of our comb states was conducted using the Ikeda map, expanded to include the auxiliary ring. The model is based on ref. [21], involving two coupled rings each having the same circumference (L), with the FSR difference between cavities emulated by using a different group index. The two coupling regions (bus waveguide-to-ring and ring-to-ring) are separated by distance of $L/2$. Thus, a full roundtrip of simulation involves (1) coupling between bus waveguide and main ring, (2) nonlinear propagation in both rings over a distance $L/2$, (3) coupling between main ring and auxiliary ring and (4) nonlinear propagation in both rings over a distance $L/2$.

The bus waveguide-to-ring and ring-to-ring transmissions are calculated through coupled-mode theory by using the corresponding coupling matrices expressed as

$$\begin{bmatrix} A_{\text{out}} \\ A^{(a)} \end{bmatrix} = \begin{bmatrix} \sqrt{1-\theta_1} & i\sqrt{\theta_1} \\ i\sqrt{\theta_1} & \sqrt{1-\theta_1} \end{bmatrix} \begin{bmatrix} A_{\text{in}} \\ A'^{(a)} \end{bmatrix},$$

and

$$\begin{bmatrix} A^{(a)} \\ A^{(b)} \end{bmatrix} = \begin{bmatrix} \sqrt{1-\theta_2} & i\sqrt{\theta_2} \\ i\sqrt{\theta_2} & \sqrt{1-\theta_2} \end{bmatrix} \begin{bmatrix} A'^{(a)} \\ A'^{(b)} \end{bmatrix},$$

respectively, where $\theta_1 \approx \frac{2\pi f_0}{\text{FSR} \cdot Q_{\text{ex}}}$ and $\theta_2 \approx (\frac{\kappa}{\text{FSR}})^2$ describe the portion of power coupled between waveguides, with f_0 being the pump frequency. The superscript, a and b, correspond to main cavity and auxiliary cavity, respectively. The nonlinear propagation in each microresonator is described by the nonlinear Schrödinger equation (NLSE),

$$\left(\frac{\partial}{\partial z} + \frac{\alpha^{(a,b)}}{2} + i\delta^{(a,b)} + d^{(a,b)}\frac{\partial}{\partial T} + i\frac{\beta_2^{(a,b)}}{2}\frac{\partial^2}{\partial T^2} - \frac{\beta_3^{(a,b)}}{6}\frac{\partial^3}{\partial T^3} - i\gamma^{(a,b)}|A^{(a,b)}|^2 \right) A^{(a,b)} = 0,$$

where $\alpha^{(a,b)}$ is the propagation loss, $d^{(a,b)}$ describes the pulse walk-off between the two cavities using the main cavity as reference, $\beta_2^{(a,b)}$ is the group velocity dispersion, $\beta_3^{(a,b)}$ is the third-order dispersion and $\gamma^{(a,b)}$ is the nonlinear Kerr parameter. The propagation distance is denoted by z, and T is the reference time given by $T = t - \frac{z}{\text{FSR}^{(a)}L}$, where t is time. Mode a is used as a reference for the walk-off, such that $d^{(a)} = 0$ and $d^{(b)} = \frac{1}{\text{FSR}^{(a)}L} - \frac{1}{\text{FSR}^{(a)}L}$. The parameter $\delta^{(a,b)}$ describes the accumulated phase per unit length with regards to the pump laser, which can be transformed into frequency detuning via $\Delta f^{(a,b)} = \text{FSR}^{(a,b)}\delta^{(a,b)}L/(2\pi)$. In each round trip, a CW pump along with quantum noise consisting of one photon per spectral bin with random phase is coupled to the ring. The nonlinear propagation is solved numerically using the Runge-Kutta method in the interaction picture[39].

The model was used to simulate the DS comb states in Fig. 2. The parameters used in these simulations were based on measurements of device 1, with the auxiliary resonance blue detuned 2.5 GHz from main resonance ($\Delta f^{(b)} - \Delta f^{(a)} = 2.5$ GHz) and $\kappa/(2\pi) = 730$ MHz ($\theta_2 = 0.0004072$). The main and

auxiliary cavities are both set to have a 100 micron radius with FSR$^{(a)}$=227.33 GHz and

FSR$^{(b)}$=236.84 GHz, $\beta_2^{(a,b)}$=66 ps^2/km, $\beta_3^{(a,b)}$=−0.9 ps^3/km and $\gamma^{(a,b)}$=1.1 (Wm)$^{-1}$. The intrinsic Q used in

the simulations is slightly lower (6.6 million, $\alpha^{(a,b)}$=1.2735 m^{-1}) than the measured mean intrinsic Q, but

within experimental uncertainty. The coupling rate between bus and ring is θ_1=0.0014. The laser

detuning is estimated only qualitatively, by comparing the simulated and measured power

transmission/conversion traces. A quantitative measurement of the detuning was not conducted due

to challenges with distinguishing between thermal and Kerr nonlinearities. Details for producing the

existence map of Fig. 2a are provided in the Supplementary Information.

The DS simulated in Fig. 4 was based on device 2. The parameters used in these simulations were

based on measurements of device 2, with $\kappa/(2\pi)$=470 MHz (θ_2=0.000794) and pump set to 17.8 mW.

The main and auxiliary cavities are both set to have a 217 micron radius with FSR$^{(a)}$=104.8 GHz and

FSR$^{(b)}$=106.9 GHz, $\beta_2^{(a,b)}$=65 ps^2/km, $\beta_3^{(a,b)}$=−0.5 ps^3/km and $\gamma^{(a,b)}$=1.1 (Wm)$^{-1}$. The intrinsic Q is set to

5.6 million ($\alpha^{(a,b)}$=1.5117 m^{-1}) and the coupling rate between bus and ring was θ_1=0.0038. The

detunings of both main and auxiliary resonators were treated as free parameters. They were set such

that the auxiliary resonance had a fixed offset of 0.65 GHz from main resonance ($\Delta f^{(b)}$−$\Delta f^{(a)}$=0.65

GHz). The laser was tuned into resonance from the blue side, stopping when red detuned by

$\Delta f^{(a)}$=333.59 MHz from main resonance and $\Delta f^{(b)}$=983.59 MHz from auxiliary resonance.

Finally, the DS simulated in Fig. 5 was also based on device 1. The coupled pump power was set to

2.5 mW with the auxiliary resonance detuned 3 GHz from the main resonance. The comb is initiated

by tuning into the main resonance from the blue side. The laser stops when it is red detuned by

$\Delta f^{(a)}$=231.5 MHz from main resonance and $\Delta f^{(b)}$=3.2315 GHz from auxiliary resonance.